LATERAL AND VERTICAL TRENDS OF PREFERRED FLOW PATHWAYS ASSOCIATED WITH BIOTURBATED CARBONATE: EXAMPLES FROM MIDDLE TO UPPER JURASSIC STRATA, CENTRAL SAUDI ARABIA

HASSAN ELTOM AND STEPHEN T. HASIOTIS
Kansas Interdisciplinary Carbonates Consortium (KICC), Department of Geology, University of Kansas, Lawrence, Kansas 66045 USA
e-mail: heltom@ku.edu

ABSTRACT: Shallow to deeply penetrating bioturbation by organisms on carbonate shelves can alter the original depositional texture of carbonate sediments, rearrange and modify the primary porosity and permeability patterns, and effectively increase the overall flow properties in multiple intervals. To explore the impact of bioturbation on reservoir quality and its spatial and vertical patterns, this study examined sedimentologically, ichnologically, and geostatistically ubiquitous bioturbated strata throughout outcrops of the Middle Jurassic Tuwaiq Mountain Formation and Upper Jurassic Hanifa Formation in central Saudi Arabia. Each lithofacies within the studied intervals had an ichnofabric index (ii) range from nonbioturbated (ii1) to beds completely homogenized by bioturbation (ii6). Most important was the occurrence of laterally extensive (>5 km) Glossifungites Ichnofacies, which represent firmgrounds with ii2 to ii5. These Glossifungites Ichnofacies are composed of complex and deep, three-dimensional *Thalassinoides* burrow networks (TBN) in mud-dominated lithofacies. These TBN have pore systems that consist of (1) open and partially open macropores (size of several centimeters), and (2) interparticle and moldic pores within the burrow filling, which consists of peloids, skeletal grains, and coated grains in a grain-dominated packstone texture. The TBN pore system, which typically penetrates the entire extent of the mud-dominated bioturbated beds, provides permeability pathways in an otherwise less permeable medium. Outcrop data and three-dimensional models suggest that these permeable pathways can contribute to overall reservoir flow in three ways: (1) TBN beds contribute to the overall reservoir flow as a single flow unit if bound above and below by impermeable beds (e.g., lateral flow in vertical well). (2) TBN breach the bed boundaries and, thus, connect above and below into more porous, more permeable grainy beds, providing overall reservoir connectivity for the carbonate reservoir and contributing to vertical and lateral flow. (3) TBN beds connect otherwise laterally compartmentalized reservoirs and contribute to vertical flow. Controls on the lateral and vertical variability of the TBN in the study area can be attributed to changes in water chemistry of the depositional environments, which are likely linked to global and local controls. This spatial and temporal relationship impacts the lateral and vertical distribution of flow properties of TBN strata in bioturbated reservoirs. Understanding such relationships is critical for secondary and tertiary recovery of oil by water flooding because such relationships can provide a prediction about the trend of vertical and lateral flow properties.

KEY WORDS: reservoirs, Hanifa Formation, ichnology, *Thalassinoides*, Cruziana Ichnofacies, Glossifungites Ichnofacies

INTRODUCTION

The relationship between biological activities and depositional texture in sedimentary rocks is well documented (e.g., Droser and Bottjer 1986, Pemberton and Gingras 2005, Hasiotis and Platt 2012). This relationship can prove challenging to interpret, however, because of the inherited geometrical complexities in burrow attributes—orientation, geometry, interconnectivity, and density—and burrow medium (i.e., substrate) (e.g., Ekdale et al. 1984; Hasiotis 2002; Gingras et al. 2012; La Croix et al. 2012, 2013). Although the modifications to the depositional texture of the burrow medium resulting from bioturbation are relatively well understood (e.g., Pemberton and Gingras 2005, Counts and Hasiotis 2009, Halfen and Hasiotis 2010, Tonkin et al. 2010, Gingras et al. 2012, Hasiotis and Platt 2012, Bayet-Goll et al. 2017, Leaman and McIlroy 2017), the spatial and temporal variation of such modification and its effect on lateral and vertical variations of petrophysical properties are less well constrained (La Croix et al. 2012; Baniak et al. 2013, 2014, 2015). Understanding such lateral and vertical trends is important because it has direct implications for understanding reservoir quality of bioturbated carbonate reservoirs.

Previous work has shown that bioturbation can play a major role in modifying depositional texture, alter the primary porosity, and provide permeability enhancement for carbonate reservoirs and aquifers (e.g., Cunningham et al. 2009, Tonkin et al. 2010, Gingras et al. 2012, La Croix et al. 2013, Baniak et al. 2015). The Biscayne aquifer of South Florida, for example, has open *Ophiomorpha* shafts that resulted in substantial interburrow macropores. These macropores provide high permeability (>5 Darcies) for the Biscayne aquifer in an area extending 345 km^2 (Cunningham et al. 2009). Another example of enhanced porosity and permeability by bioturbation is the Cretaceous Ben Nevis Formation in the Jeanne d'Arc Basin, offshore Newfoundland, Canada (Tonkin et al. 2010), where there is an increase in permeability by as much as 600% and significantly enhanced reservoir quality (Tonkin et al. 2010). Thus, mapping of lateral and vertical bioturbation patterns can enhance understanding of the impact of bioturbation on the formation of preferred flow pathways, and hence permeability.

Extensively bioturbated strata dominate outcrops of the Middle Jurassic Tuwaiq Mountain Formation and Upper Jurassic Hanifa Formation in central Saudi Arabia (e.g., Hughes et al. 2008). These outcrops provide vertical and lateral exposures that offer a unique opportunity for a detailed description of sedimentological, ichnological, and stratigraphic features in strata equivalent to subsurface bioturbated reservoirs. The bioturbated strata of these outcrops are dominated by the Glossifungites Ichnofacies, composed of complex and deep, three-dimensional *Thalassinoides* burrow networks (TBN) within weakly to strongly bioturbated, fine-grained deposits that after bioturbation become firmgrounds (e.g., Gingras et al. 2012). These TBN occur as exceptionally preserved boxwork patterns composed of interconnected vertical to subvertical shafts and horizontal to subhorizontal tunnels in outcrop. Multiple generations of TBNs

Carbonate Pore Systems: New Developments and Case Studies
DOI: 10.2110/sepmsp.112.05
SEPM Special Publication No. 112, Copyright © 2019
SEPM (Society for Sedimentary Geology), ISBN 978-1-56576-364-7, eISBN 978-1-56576-365-4, p. 126–140.

produce multiple, interpenetrated boxwork networks, where burrows may appear as individual elements but rather are part of one or more TBN.

In this context, the objectives of this study were to: (1) document the spatial and temporal variation in TBN of shallow carbonate strata; (2) determine the impact of TBN on changing sediment texture and potential preferred flow pathways; and (3) understand how these preferred flow pathways vary laterally and vertically to predict trends for hydrocarbon exploration and development. Results provide predictions for hydrocarbon exploration and development by understanding trends in petrophysical properties that are associated with bioturbated carbonate strata.

GEOLOGICAL BACKGROUND AND METHODS

Geological Setting

The Middle to Upper Jurassic carbonate succession of central Saudi Arabia was deposited in the southern margin of the Tethys Ocean (Fig. 1A) and represents an epeiric sea on a broad, shallow-marine shelf (e.g., Al-Husseini 1997). The Hanifa Formation in central Saudi Arabia (Fig. 1B, C) is assigned an Oxfordian to Kimmeridgian age based on ammonites, macrofossils, and microfossils (e.g., Hughes et al. 2008). The formation includes two members: the Hawtah Member and the Ulayyah Member, both of which are third-order sequences that contain several higher-frequency sequences (Fig. 1C; Hughes et al. 2008).

Recent investigations have subdivided the Hanifa Formation into several paleoenvironmental settings, ranging from nearshore to deep intrashelf basin (Fig. 2A; Hughes et al. 2008; Eltom et al. 2017, 2018; Fallatah and Kerans 2018). Organic-rich deposits that accumulated mostly in calm, deep-water marine settings of this basin (Fig. 2A; Droste 1990) pass updip towards the basin flanks to lithofacies interpreted to indicate higher energy than those in the depocenter of the basin (Hughes et al. 2008). Details of lithofacies and their stratigraphic patterns in the Haifa Formation are available in Eltom et al. (2017, 2018) and Fallatah and Kerans (2018).

Deposition of the Hanifa Formation occurred throughout vigorous marine upwelling that co-occurred with the development of intrashelf basins in the Arabian Plate (Droste 1990; Cantrell et al. 2014; Eltom et al. 2017, 2018). These conditions led to the enhancement of organic productivity and the deposition of extensive, organic-rich strata with an average total organic carbon (TOC) value of ∼3% (reaching up to ∼13%). Eltom et al. (2017) presented high-resolution, carbon and oxygen isotopic data of the Hanifa Formation and suggested that the trends in these isotopic values could have been affected locally by the concurrent development of organic productivity.

Study Area

This study investigated strata that contain TBN in the Hanifa Formation in three outcrop sections in central Saudi Arabia (Fig. 2). These outcrop sections (from downdip to updip) are Wadi Nisah (WN), Diplomatic Quarter (DQ), and Jubal Abakkayn (JA) (Fig. 2). In the WN section, the Hanifa Formation is 109 m thick, although there are two covered intervals of ∼14 m total (Fig. 2; Eltom et al. 2017). The DQ section (∼85 m thick) represents a road cut with fresh, unweathered rocks, the same as that studied by Hughes et al. (2008) and Eltom et al. (2018) for paleontological characterization and geochemical chemical (isotopic) signatures (Fig. 2). The JA section (Fig. 2) is the type section of the Hanifa Formation and was described initially by Powers et al. (1966). This section has ∼82-m-thick strata, with the lower half of the formation exposed along a road cut; an ∼17 m section of the lower part of the Ulayyah Member is covered (Fig. 2). About a 28-m-thick interval of the Ulayyah Member of the Hanifa Formation that overlies this covered interval is exposed as a cliff.

Methodology

The Hanifa Formation was described in the three outcrop sections (WN, DQ, and JA; Fig. 2) by its lithological and ichnological characteristics and stratigraphic stacking pattern. In total, 260 rock samples were collected for thin sections and analyzed for microfacies and micropaleontology. Petrographic data were used along with field observations to interpret the depositional environments. Results of laboratory and field observations are reported in the lithological log profiles (Fig. 2).

Trace fossils were identified according to their architectural and surficial morphologies and fill pattern (e.g., Hasiotis and Mitchell 1993). Bioturbation intensity of the strata was measured using the ichnofabric index (ii) of Droser and Bottjer (1986) to describe bioturbation and TBN intensity in outcrop (ii1 = 0; ii2 = 1–10%; ii3 = 10–40%; ii4 = 40–60%; ii5 = 60–100%; ii6 = >100%) of the Hanifa and Tuwaiq Mountain formations, which was evaluated in the three studied outcrop sections and plotted as vertical profiles. The ii measures the degree of disburbance of the original sedimentary fabric resulting from bioturbation (Droser and Bottjer 1986). In other words, ii is a measure of the bioturbation intensity that disrupts the original depositional fabric.

To construct geostatistical models for lithofacies and their burrow intensity in the study area, we used data from three prvious works:

1. Hughes et al. (2008) studied the Hanifa Formation in outcrop and subsurface using several wells and outcrop sections. They provided a two-dimensional (2D) interpreted map of the upper Hanifa Formation for an area that includes most of the oilfields in eastern Saudi Arabia and outcrops in the central part of Saudi Arabia, based on these well data and outcrop sections (including our study area).
2. Eltom et al. (2017, 2018) studied lithofacies and carbon isotope data of the Hanifa Formation in two sections that represent updip and downdip depositional profiles. The analysis identified six mappable units with distinct isotopic signatures between the updip and downdip sections, which helped stratigraphic correlations in the Hanifa Formation.
3. Fallatah and Kerans (2018) studied lithofacies of the Hanifa Formation and the underlying Tuwaiq Mountain Formation in 15 locations and provided stratigraphic data and cross sections of these sections. They provided 2D lithofacies distribution maps of the Hanifa Formation in the study area.

By integrating these data, we interpolated between outcrop sections and constructed 160 interpreted, 2D conceptual models of the Hanifa Formation, each representing a stratigraphic interval of ∼0.75 m (Fig. 3A, B). These 2D conceptual models were converted to geocellular models and stacked together to build a three-dimensional (3D) facies model of the Hanifa Formation (Fig. 3C).

This 3D facies model has a limitation as a reservoir analog model because of the small number and scattering of the measured sections that we used in the modeling process. The model, however, is an excellent conceptual perspective of facies distribution in the Hanifa Formation. The advantage of this 3D model is that by having a conceptual 3D facies distribution in a geocellular model, we can distribute the intensity of bioturbation in a 3D grid using facies-based modeling.

The modeling process in this study included four steps:

1. The first step was to define the modeling area. We generated a polygon in Google Earth for the modeling area in central Saudi Arabia (Fig. 3A), an area that included all the studied sections from previous work. This polygon extended 200 km in the north–south direction and 130 km in the east–west direction (Fig. 3A). The

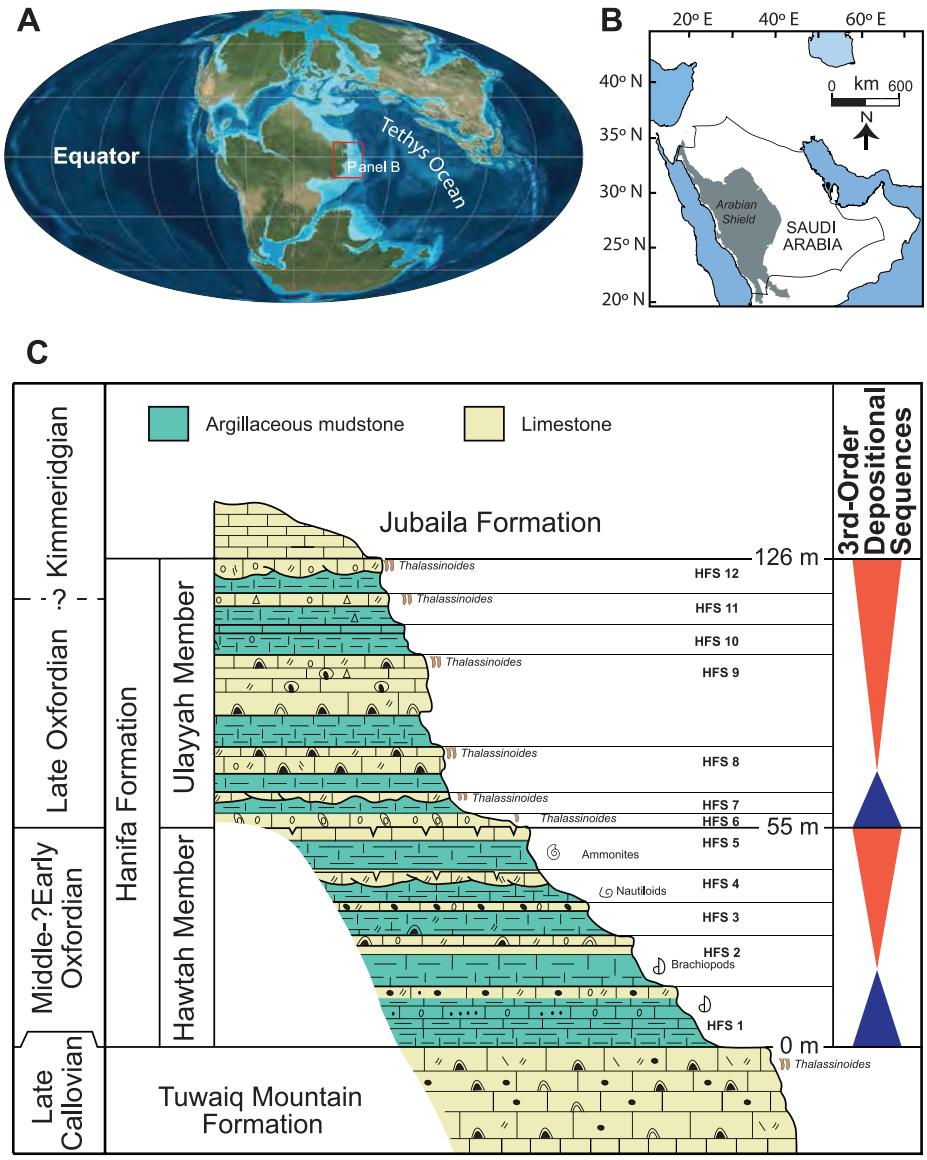

FIG. 1.—Study area. **A)** Paleogeographic map of the Arabian Plate (red box) at the southern margin of the Tethys Ocean. **B)** Map of Saudi Arabia, where studied interval is exposed. **C)** Stratigraphy of the Hanifa Formation, the underlying Tuwaiq Mountain Formation, and the overlying Jubaila Formation in central Saudi Arabia (modified from Al-Husseini 1997).

polygon was exported to Petrel™ 2016 as a shapefile and was used to construct surfaces for a 3D structural grid of our models (Fig. 3B).

2. The second step was to construct a 3D grid for the modeling area. We constructed a 3D structural grid consisting of cells with 2D horizontal dimensions of 1 km by 1 km. We used 160 layers, where each was ~0.75 m. In this 3D structural grid, four east–west normal faults were inserted on top of locations in the polygon that showed wadis (seasonal channels filled with rainfall) in Google Earth (Fig. 3B). Inserting such structural features in our model provided a more realistic visualization and analogy for the Hanifa and upper Tuwaiq Mountain reservoirs.
3. The third step included lithofacies modeling. Lithofacies distribution was generated manually (no modeling algorithms were used) in each one of the 160 2D layers based on understanding of spatial variation in the field, guided by outcrop data from previous studies (Hughes et al. 2008; Eltom et al. 2017, 2018; Fallatah and Kerans 2018). Although time-consuming, manual construction of lithofacies in these 2D layers ensured that no software errors were introduced to the models.
4. The fourth step included burrow-intensity modeling. From field observations, each lithofacies (13 lithofacies) was given a range of burrow intensity (Table 1). Using these ranges, we stochastically distributed burrow intensity in the 3D grid by a facies-based technique. The stochastic distribution was created by a Gaussian random function simulation (GRFS) algorithm in Petrel 2016. The primary input for the GRFS was the 3D facies model that we constructed earlier in steps 1 to 3. GRFS stochastically distributed the defined range of burrow intensity in each lithofacies separately in the 3D facies model.

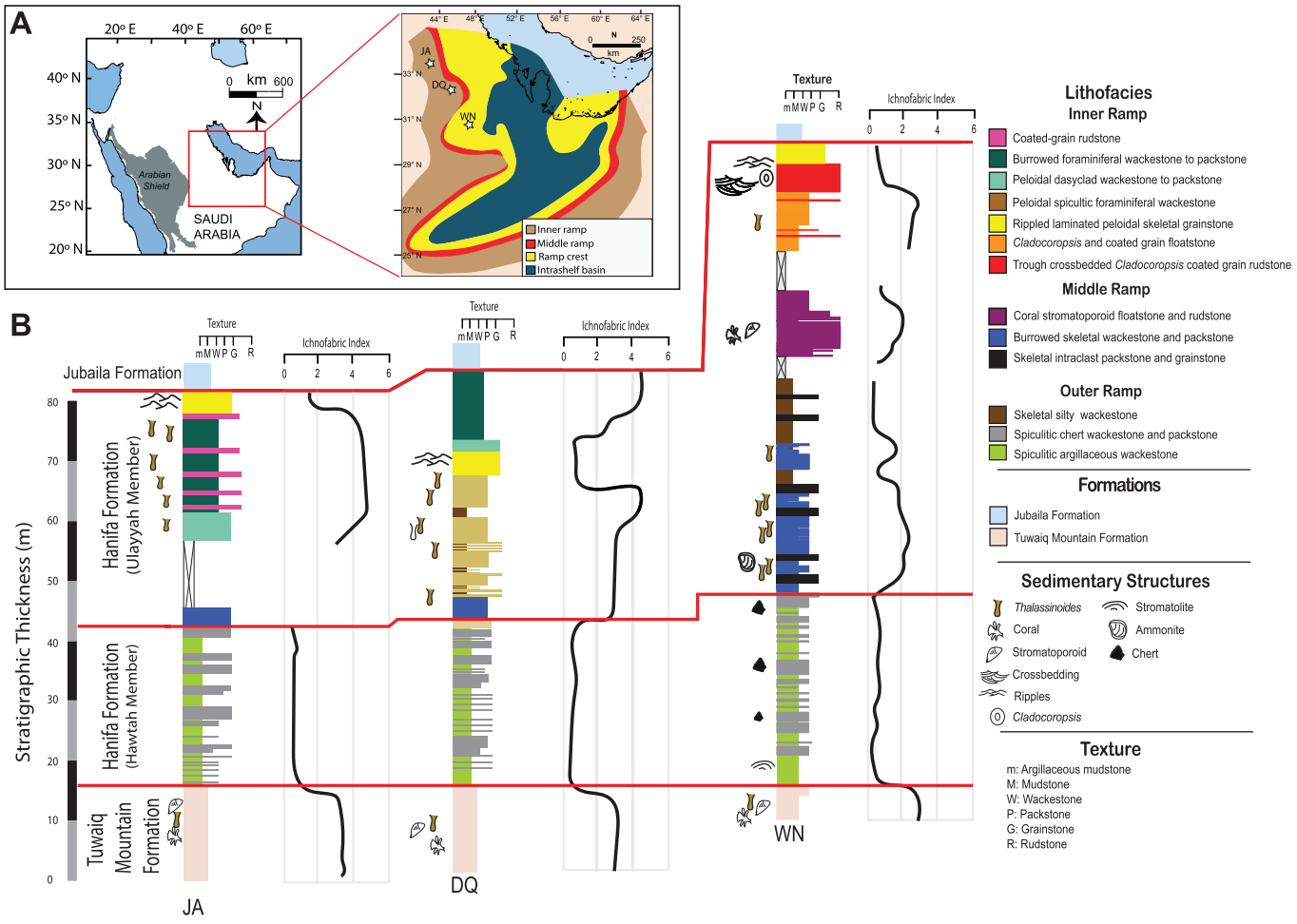

FIG. 2.—Facies, environments of deposition, and stratigraphy. **A)** Map of depositional environments of the Hanifa Formation in central Saudi Arabia as interpreted by Hughes et al. (2008). Note locations of the three studied outcrops (Wadi Nisah, WN; Diplomatic Quarter, DQ; and Jubal Abakkayn, JA) and their geographic locations regarding the intrashelf basin in the eastern part of the Arabian Plate. **B)** Stratigraphic logs of the three studied outcrop sections generated by integrating outcrop observations and thin-section descriptions from the study succession.

RESULTS

Lithofacies

Observations from the outcrop sections of the Hanifa Formation and previously published data in the study area (Fig. 2) (e.g., Al-Husseini 1997, Hughes et al. 2008, Eltom et al. 2017) provide the stratigraphic and sedimentological framework for this study. Accordingly, the Hanifa Formation was divided into 13 lithofacies (LF) (Table 1) grouped into three lithofacies associations (LFA). The underlying Tuwaiq Mountain Formation and the overlying Jubaila Formation were considered to represent individual lithofacies units, although their lithological composition may vary laterally. The three LFA of the Hanifa Formation represent deposition in an eastward-dipping ramp environment (see Table 1 in Eltom et al. 2018).

1. LFA 1 (outer ramp): (LF 1) spiculitic argillaceous wackestone; (LF 2) spiculitic chert wackestone and packstone; and (LF 3) skeletal silty wackestone.
2. LFA 2 (middle ramp): (LF 4) skeletal intraclast packstone and grainstone; (LF 5) burrowed skeletal wackestone and packstone; and (LF 6) coral-stromatoporoid floatstone and rudstone.
3. LFA 3 (inner ramp): (LF 7) trough cross-bedded, *Cladocoropsis*, and coated grain rudstone; (LF 8) *Cladocoropsis* and coated grain floatstone; (LF 9) ripple-laminated peloidal skeletal grainstone; (LF 10) peloidal spiculitic foraminiferal wackestone; (LF 11) peloidal dasyclad wackestone and packstone; (LF 12) burrowed foraminiferal wackestone to packstone; (LF 13) coated grain rudstone.

Trace Fossils

The trace fossils in the Hanifa Formation (Figs. 4, 5) include *Chondrites*, *Conichnus*, *Ophiomorpha*, *Phycodes*, *Rhizocorallium*, *Schaubcylindrichnus*, *Skolithos*, *Taenidium*, *Teichichnus*, and *Thalassinoides*. Most of the trace-fossil assemblages indicate either a distal Skolithos and proximal Cruziana Ichnofacies. The most dominant occurring ichnotaxon in heterozoan and photozoan deposits is *Thalassinoides*. Details of the

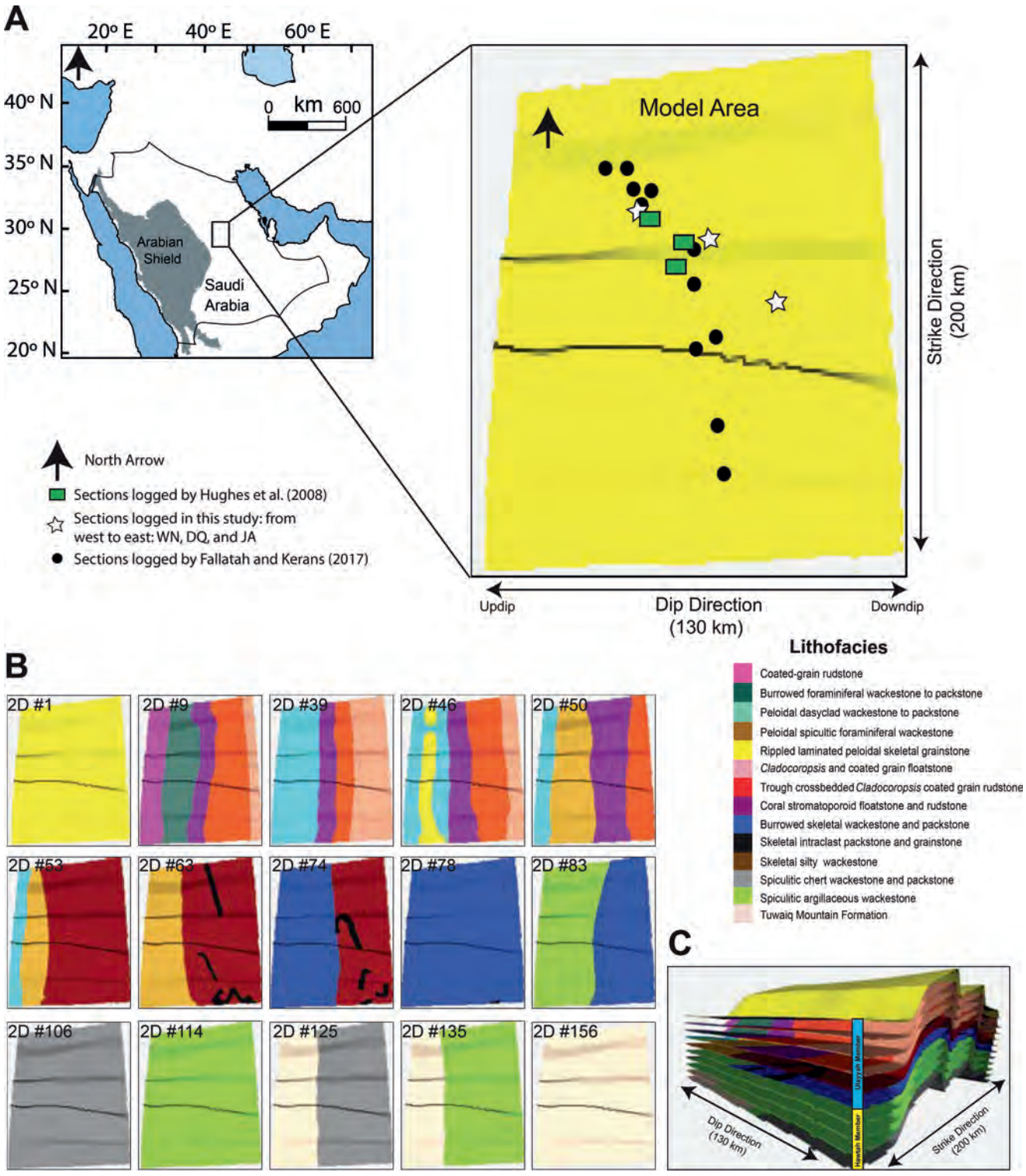

FIG. 3.—Model construction workflow: **A)** Map showing polygon surrounding the modeled area. **B)** Selected 2D interpreted conceptual models used to build the 3D facies. Note that the 2D models were labeled 1 to 160 from top (top of the Hanifa Formation) to bottom (bottom part of the Tuwaiq Mountain Formation). The number at the corner of each 2D model represents its label. **C)** 3D visualization of selected 2D interpreted conceptual models showing how they were stacked to build the 3D facies model.

TABLE 1.—Lithofacies, lithofacies association, ichnofabric index, and burrow intensity.

Lithofacies association	Lithofacies number	Lithofacies name	Ichnofabric index	Burrow intensity (%)
LFA 1	F13	coated grain rudstone	1	0
	F12	burrowed foraminiferal wackestone to packstone	4–6	40–100
	F11	peloidal dasyclad wackestone to packstone	3–4	20–50
	F10	peloidal spiculitic foraminiferal wackestone	2–3	10–20
	F9	ripple-laminated peloidal skeletal grainstone	1	0
	F8	*Cladocoropsis* and coated grain floatstone	2–3	10–20
	F7	trough cross-bedded *Cladocoropsis* coated grain rudstone	1	0
LFA 2	F6	coral stromatoporoid floatstone and rudstone	1	0
	F5	burrowed skeletal wackestone and packstone	3–4	30–50
	F4	skeletal intraclast packstone and grainstone	2–3	10–20
LFA 3	F3	skeletal silty wackestone	1	0
	F2	spiculitic chert wackestone and packstone	1–2	0–10
	F1	spiculitic argillaceous wackestone	1	0
Tuwaiq Mountain Formation			3–4	10–30

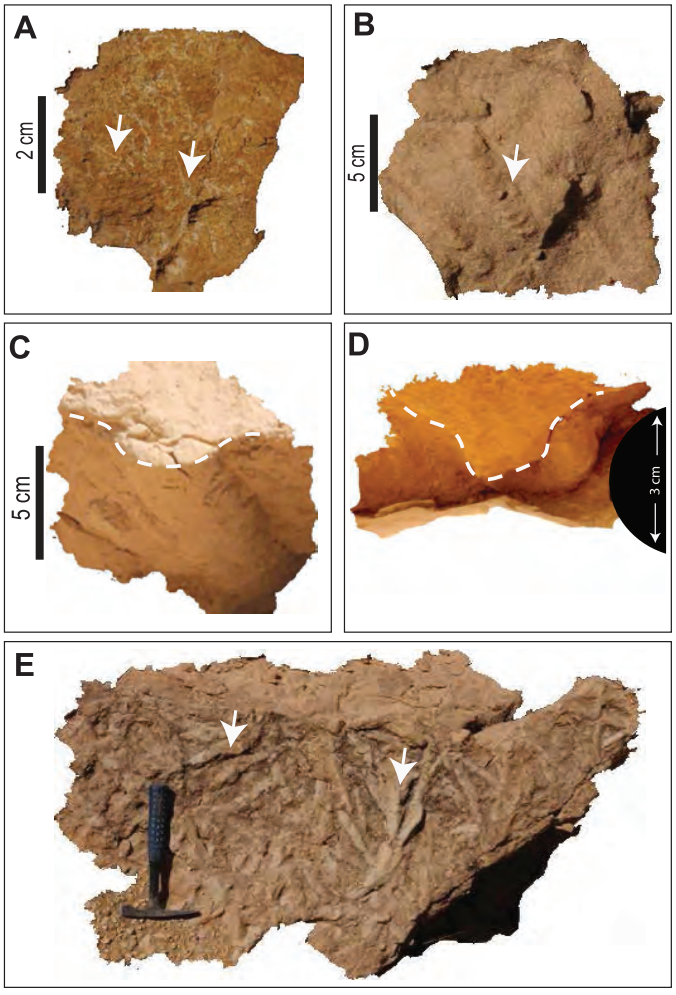

FIG. 4.—Trace fossils in the studied interval (indicated by white arrows and/or dash lines): **A)** *Chondrites*, **B)** *Taenidium*, **C)** *Teichichnus*, **D)** *Conichnus*, and **E)** *Phycodes*. Partial lens cap in C is ~3 cm.

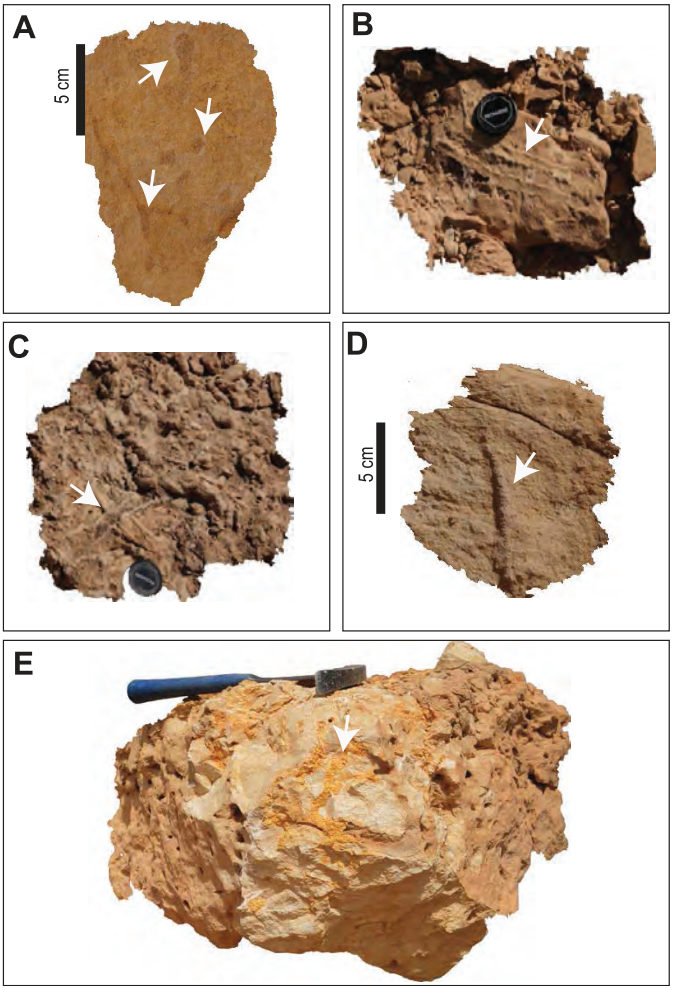

FIG. 5.—Trace fossils in the studied interval (indicated by white arrows): **A)** *Schaubcylindrichnus*, **B)** *Rhizocorallium*, **C)** *Ophiomorpha*, **D)** *Skolithos*, and **E)** *Thalassinoides*. Lens cap is 6.7 cm.

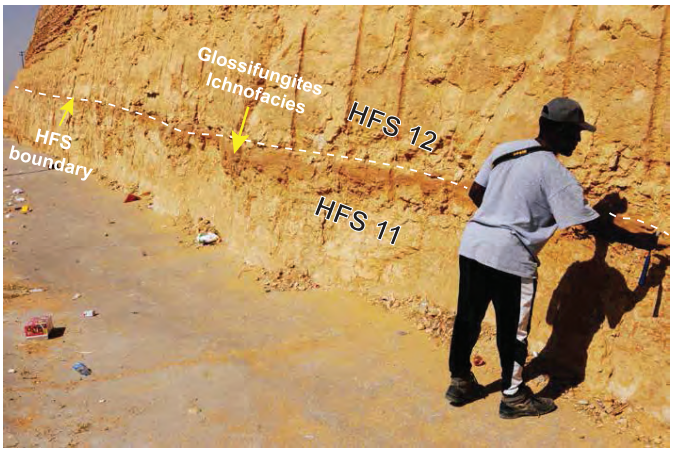

FIG. 6.—Discontinuity surface of the Glossifungites Ichnofacies marking HFS boundary at the upper part of the Ulayyah Member of the Hanifa Formation.

ichnology will be reported in a separate contribution that focuses on the ichnotaxonomy and paleoecology of the Hanifa Formation.

TBN Morphology and Pore System

The TBN of the Hanifa Formation have a range of ii2 to ii6. Laterally extensive horizons of firmgrounds of the Glossifungites Ichnofacies commonly record high-frequency sequences (HFS) boundaries that can extend for tens of kilometers (Fig. 6). Vertically, these TBN firmgrounds can: (1) be confined only within one bioturbated bed (Fig. 7A); (2) breach bed boundaries above the bioturbated beds and connect to porous and permeable grain-dominated beds (Fig. 7B); and (3) breach bed boundaries above and below the bioturbated bed and connect to porous and permeable grain-dominated beds (Fig. 7C).

The biogenic pores associated with TBN in the studied interval occur in three forms (Figs. 8–10). The first and most common pore type of TBN occurs as macropores in the form of open and partially open burrows (Figs. 8–10B). The 2D outcrop views of these macropores show circular shapes (Fig. 8) and have a complicated shape in 2D slices that are cut perpendicular to these outcrop views (Fig. 9). The width of these macropores ranges from 0.7 to 4.5 cm (Fig. 11), with their sizes varying laterally from downdip to updip (see the following section). The partial fillings of TBN consist of skeletal grains, peloids, and coated grains, and they have a grain-dominated packstone depositional texture with an estimated visual porosity range from 10 to 20% (Fig. 10B).

The second and third pore types of TBN, which are less common than the macropores, occur as interparticle and moldic pores in the grain-dominated packstone depositional texture of the burrow fill materials (Fig. 10C–F). The filling materials of TBN consist of skeletal grains, peloids, and coated grains (Fig. 10C–F). The difference between the second and third pore types of TBN is that the second pore type has an estimated visual porosity range from 10 to 20% (Fig. 10C–E), whereas the third pore type is entirely occluded by cement and mud and has an estimated visual porosity of 0% (Fig. 10F).

Vertical and Lateral Patterns of TBN

TBN are observed in the three studied sections. There is, however, spatial variation in bioturbation intensity and burrow size (i.e., apparent burrow diameter) among the study sections (Figs. 2, 12). Generally, these variables increase from downdip to updip, as *Thalassinoides* specimens show remarkably larger size and higher density in the JA and DQ sections (updip sections) compared to the WN section (downdip section). For example, burrows downdip have a modal diameter of 0.7 cm, increasing to almost 1.4 cm updip (maximum measured diameters up to 4.5 cm), as relative average bioturbation intensity increases from ii3 (10–40%) to ii5 (60–100%) (Fig. 2).

Bioturbation intensity and burrow size also vary vertically within each section (Fig. 2). The Upper Tuwaiq Mountain Formation and the Ulayyah Member of the Hanifa Formation have a higher bioturbation intensity of *Thalassinoides* (ii3–6) compared to the Hawtah Member (ii1, 2). This vertical change in bioturbation intensity can be linked to the vertical change in depositional style of the study succession. The high bioturbation intensity (ii3–5) in the Tuwaiq Mountain Formation corresponds to dominant photozoan depositional style (Eltom et al. 2017). The abrupt decrease in bioturbation intensity (ii1) in the overlying Hawtah Member corresponds to the presence of biosiliceous and heterozoan lithofacies (Eltom et al. 2017). The sudden increase of bioturbation intensity (ii3–6) in the overlying Ulayyah Member corresponds to changes in depositional style from biosiliceous and heterozoan back to photozoan deposition (Eltom et al. 2017).

Geological Model of Lithofacies and Burrow Intensity

The studied intervals represent complex stratigraphic units that contain various lithological compositions, sediment fabrics, textures, and depositional styles. The conceptual vertical and lateral variations in lithological characteristics are illustrated in the constructed geostatistical models (Fig. 12A). Patterns of vertical and lateral changes in burrow intensity are also illustrated in the constructed geostatistical model (Fig. 12B). These models were used to understand how bioturbation intensity and its related flow properties vary laterally and vertically.

DISCUSSION

Porosity and Permeability of TBN Beds

Previous studies on biogenic porosity and permeability (e.g., Cunningham et al. 2009, Tonkin et al. 2010, Gingras et al. 2012, La Croix et al. 2013, Baniak et al. 2015) have shown that burrows (1) can be filled with coarser materials than the burrow medium or (2) can be completely open (i.e., open pipes). These studies illustrated that in both cases, burrows provide permeability pathways, which, in some cases, reach more than five orders of magnitude higher than the burrow medium and provide excellent permeability for hydrocarbon reservoirs and water aquifers (e.g., Cunningham et al. 2009).

Although this study does not present results for permeability measurements, the TBN pore system suggests high permeable flow associated with TBN beds. The open and partially open macropores of TBN (Figs. 8–11), which are the dominant biogenic pore system in the study area, suggest high intrinsic permeability—permeability that depends only on the porous medium—for the TBN beds (possibly >5 Darcies). This suggestion is based on a comparison with similar bioturbated strata that have similar pore systems, and that have proven to have excellent permeability. For example, the *Ophiomorpha*-dominated bioturbated strata of the Biscayne aquifer, southeastern Florida (Cunningham et al. 2009), has substantial biogenic porosity. The open shafts of *Ophiomorpha* burrow networks have widths of several centimeters and lengths up to ~8 cm, resulting in centimeter-scale biogenic vuggy macropores, and these provide superpermeability (>5 Darcies) for the Biscayne

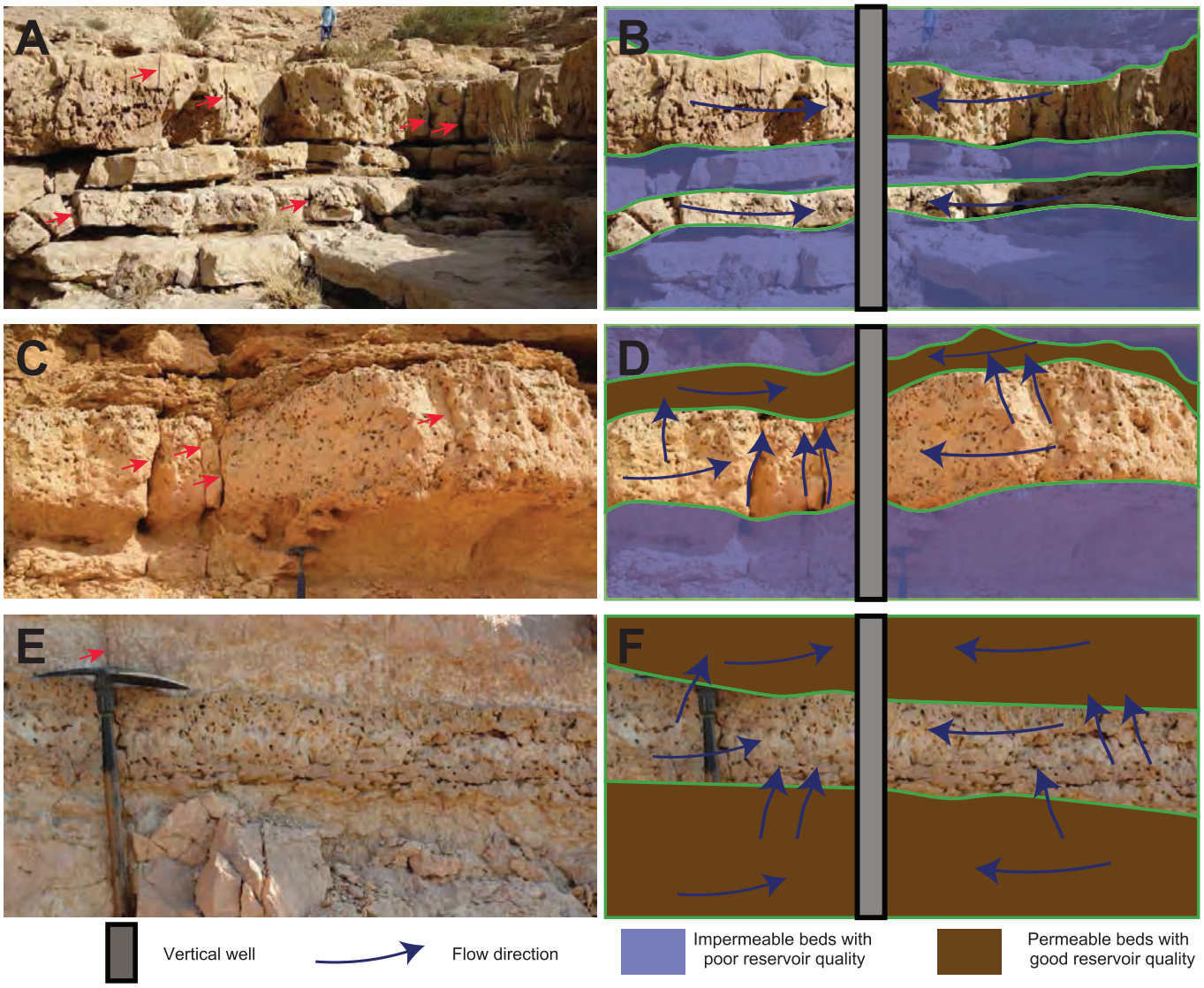

FIG. 7.—Paired uninterpreted and interpreted photographs of TBN beds and the overlying and underlying beds (red arrows show fractures). **A, B)** TBN overlies and is overlain by mud-dominated beds with interpreted poor reservoir quality. Note the expected flow comes from the TBN bed alone. **C, D)** TBN overlies mud-dominated beds with interpreted poor reservoir quality and is overlain by grain-dominated beds with interpreted good reservoir quality. Note the expected flow comes from both the TBN bed and overlying beds. In this flow unit, TBN and the grain-dominated beds are vertically connected through TBN and the fractures. **E, F)** TBN overlies and is overlain by grain-dominated beds with interpreted good reservoir quality. Note the expected flow comes from the TBN bed and grain-dominated beds. In this flow unit, TBN and the grain-dominated beds are vertically connected through TBN and the fractures.

aquifer in an area extending 345 km^2 (Cunningham et al. 2009). By inference, macropores of TBN in the studied interval in central Saudi Arabia can develop such high permeability.

The interparticle and moldic pores of the TBN filling, which occur in grain-dominated packstone depositional texture, have an estimated porosity range from 10 to 20% (Fig. 10). Typical rock textures with such porosity in the Arab-D reservoir (e.g., Mitchell et al. 1988; Meyer et al. 1996, 2000; Lindsay et al. 2006; Eltom et al. 2014), for example, could have permeability values of >100 mD (e.g., Meyer et al. 2000). Thus, the TBN that have filling materials—skeletal grains, peloids, and coated grains (Fig. 10)—with such grain-dominated packstone depositional texture can provide permeability pathways in otherwise less permeable media, and they can enhance reservoir quality of the mud-dominated firmgrounds as well. TBN with infill that have occluded interparticle and moldic pores (either by cement or mud; Fig. 10F) are less common than the TBN macropores and interparticle pores. The effect of occluded interparticle and moldic pores on the overall permeability of the TBN beds can, therefore, be neglected.

In summary, the TBN in Glossifungites Ichnofacies created an open pore system in the Hanifa Formation in central Saudi Arabia and effectively increased the overall porosity of the bioturbated strata in

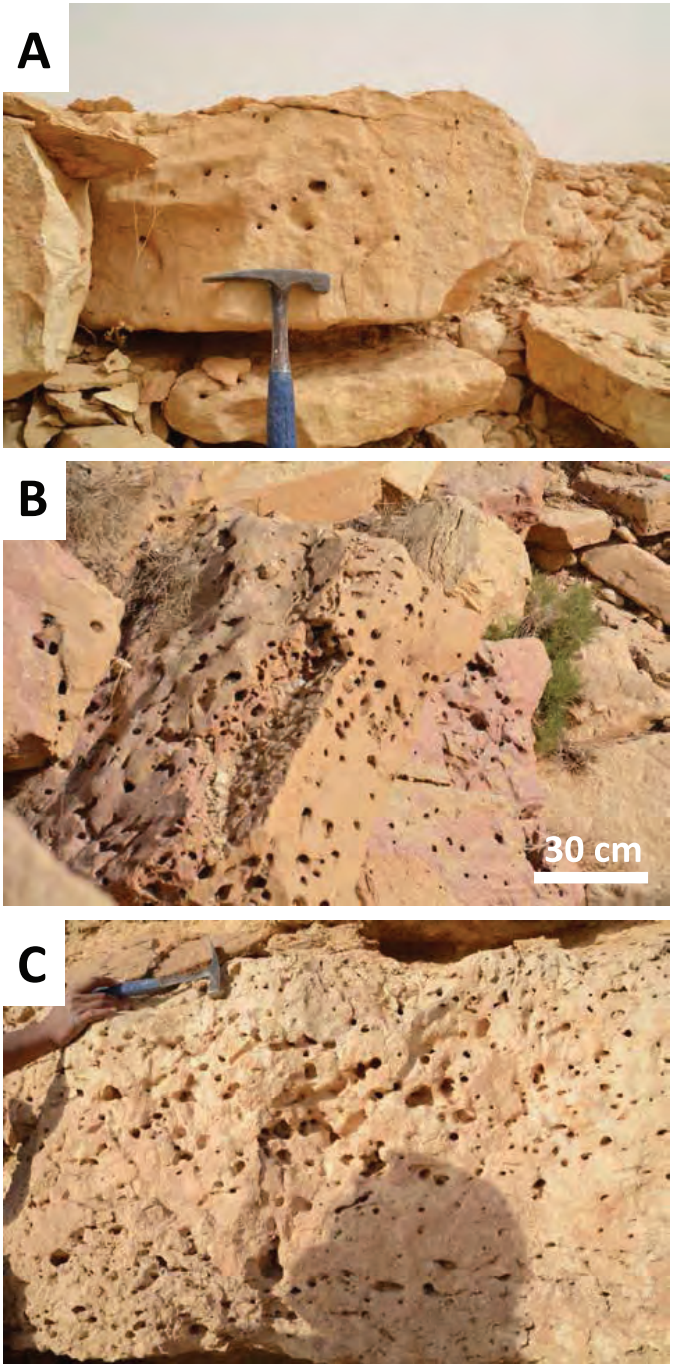

FIG. 8.—Outcrop photographs showing macropores of the TBN in the three studied locations: **A)** in WN section, **B)** in DQ section, and **C)** in JA section.

the study area. We compared the TBN pore system with the pore system of Biscayne aquifer and Arab-D reservoirs, both of which have reported permeability values. This comparison suggested that the pore system of TBN can develop excellent permeability for TBN beds—which can be >100 mD, and may reach up to several Darcies—and, thus, they provide a conduit for effective flow in bioturbated carbonate strata.

Importance of Quantification of Burrow Intensity to Predict TBN Permeability

Measuring the intrinsic permeability of such macropores as those of the TBN is challenging using the conventional laboratory methods of core analysis because of two reasons. First, the standard size of the plug samples always used for laboratory measurements is smaller than the size of these macropores. Second, laboratory methods use Darcy's law, which assumes a linear relationship between flow rate and applied hydraulic gradient. Such an assumption is not valid when applied to macropore systems, as discussed by many previous studies (e.g., Cunningham et al. 2009).

Alternatively, mathematical computations of permeability from fluid flow in pore systems using computer simulation provide an appropriate and reliable substitute to laboratory measurements. These mathematical computations of permeability suggested that the intrinsic permeability of macropores depends mainly on the connectivity of the pore system. For example, the connected macropore system of the open *Ophiomorpha* shafts has a permeability that increases with increasing burrow connectivity (Cunningham et al. 2009).

Likewise, the permeability of the TBN macropores will depend on burrow connectivity, which in turn depends on burrow intensity (e.g., La Croix et al. 2012, 2013). Generally, full connectivity (>85%) of TBN can occur in beds with as low as 12% bioturbation intensity (ii2) (La Croix et al. 2012, 2013; Eltom et al. 2018). Thus, the TBN beds can have high permeability values even at low bioturbation intensity (ii2, 3), and TBN can play an essential role in vertically and laterally connecting reservoirs zones.

The fact that burrow connectivity of TBN correlates with burrow intensity implies that burrow intensity can mirror the intrinsic permeability of TBN. This relationship can further imply that superpermeability can be generated along TBN with high intensity (Cunningham et al. 2009; Eltom et al. 2018). Thus, quantification of burrow intensity can provide a means to predict TBN permeability in bioturbated strata and their effective flow.

Controls on Vertical and Lateral Variation of TBN

To understand the effect of bioturbation on carbonate reservoir connections, it is essential to recognize the controls on the vertical and lateral variations of bioturbation intensity in the host strata. Our field observations included: (1) an upward decrease in bioturbation intensity from the Tuwaiq Mountain Formation to the Hawtah Member of the Hanifa Formation; (2) an upward increase in bioturbation intensity in the Hanifa Formation from the Hawtah to Ulayyah members; and (3) an increase in bioturbation intensity within the Ulayyah Member from bottom to top in the mud-dominated lithofacies of the updip strata. There is also a lateral increase in bioturbation intensity in the mud-dominated lithofacies of the upper part of the Ulayyah Member from downdip to updip.

These vertical and lateral trends can be linked to global and local controls, as suggested by Eltom et al. (2017) for the depositional styles of the Hanifa Formation. This deposition could reflect the interaction between global and local paleogeographic and paleoceanographic controls. Globally, the time of the deposition of the lower member of the Hanifa Formation—the Hawtah Member, late to middle Oxfordian (Hughes et al. 2008)—was characterized by poor marine circulation. The Tethys Ocean at this time was wholly isolated from the Pacific and Atlantic oceans (e.g., Gradstein et al. 1991, Louis-Schmid et al. 2007, Alberti et al. 2012), and there was a global crisis in carbonate platform development (e.g., Wierzbowski 2002). This crisis of carbonate productivity was coupled with increasing rates of biosiliceous sediments (radiolarites, sponge spicules, and chert), which have been

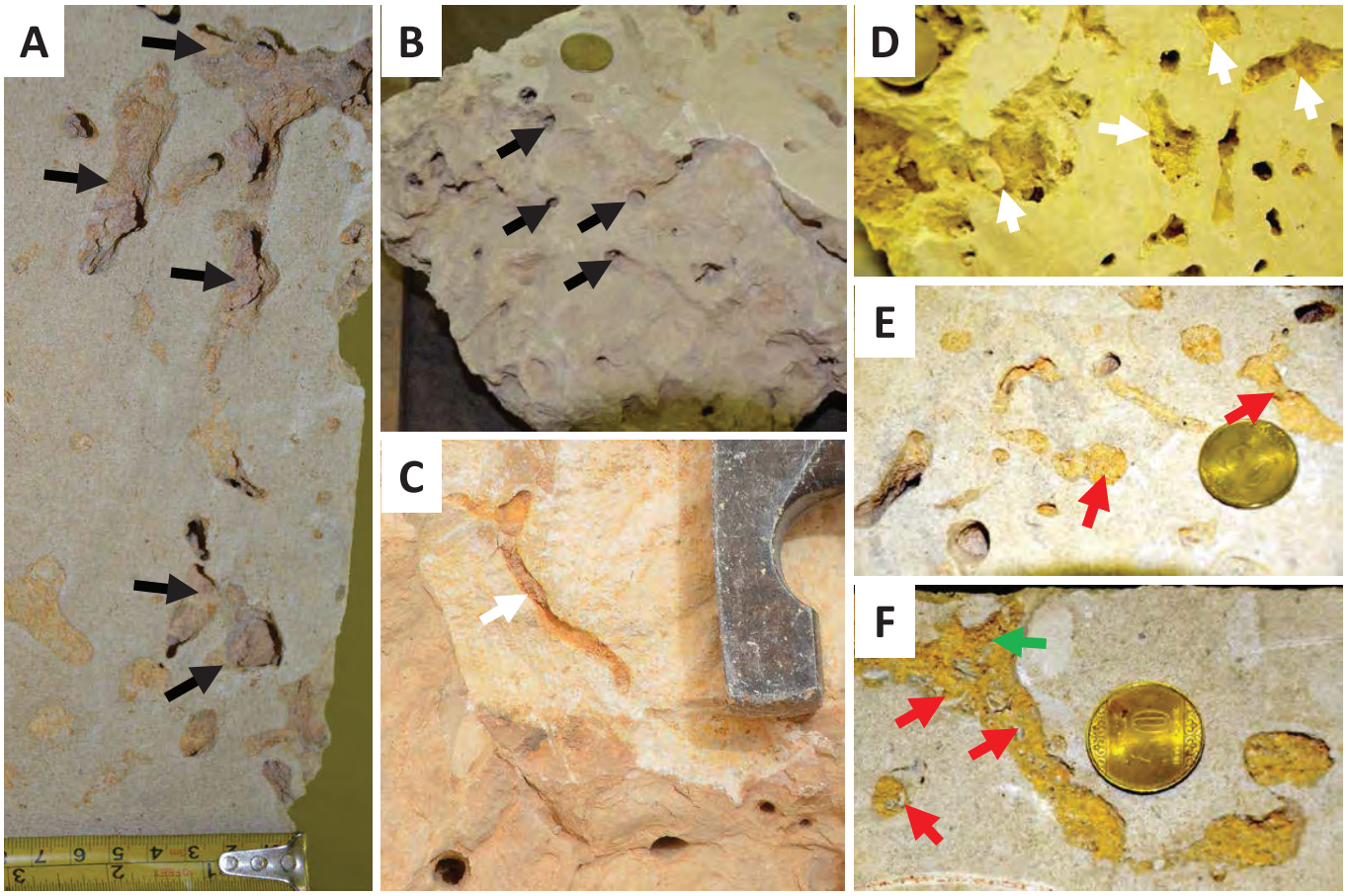

FIG. 9.—Photographs showing macropores of the TBN in slabbed samples: **A, B)** open shafts of the TBN (black arrows), **C, D)** partially filled shafts of the TBN (white arrows), and **E, F)** burrow filling of the TBN (green arrow indicates coated grains, whereas red arrows indicate skeletal grains).

globally documented (see synthesis in De Wever et al. 2014). Similar biosiliceous deposits within the studied succession (in WN section) were documented, and their accumulation was related to active marine upwelling in the Arabian Plate during middle Oxfordian time (Eltom et al. 2017). Locally, the deposition of middle Oxfordian strata occurred during a period of active marine upwelling that coincided with the formation of intrashelf basins in the Arabian Plate (Droste 1990, Cantrell et al. 2014, Eltom et al. 2017). This unique convergence of global and local factors resulted in enhanced organic productivity and the deposition of organic-rich strata—the Hawtah Member of the Hanifa Formation in the intrashelf basins—with an average TOC value of ~3% (but reaching up to ~13%), implying elevated marine productivity and abundant organic carbon (Droste 1990, Cantrell et al. 2014). Marine productivity usually results in lower dissolved oxygen concentrations in the water. The lowering of dissolved oxygen probably limited bioturbation by infaunal (i.e., endobenthic) burrowers (e.g., Reolid and Betzler 2018) and likely reduced reservoir connectivity by burrows among Hawtah Member beds.

In contrast, the late Oxfordian time witnessed an opening of two seaways among the Pacific, Atlantic, and Tethys oceans (Gradstein et al. 1991, Louis-Schmid et al. 2007, Alberti et al. 2012). The first seaway connected the northern Tethys Ocean with the central Atlantic and Pacific oceans and is referred to as the Hispanic Corridor (e.g., Gradstein et al. 1991, Louis-Schmid et al. 2007, Alberti et al. 2012). The second seaway connected the southern Tethys Ocean with the southern Atlantic and Pacific oceans and is referred to as South African Seaway (e.g., Alberti et al. 2012). The time of opening of these seaways corresponded to long-term, sea-level rise (Hallam 2001), which facilitated oceanic current movements within these seaways, and resulted in a major reorganization of waters among the Tethys, Atlantic, and Pacific oceans. This current reorganization enhanced carbonate production by creating suitable environments for carbonate producers (e.g., Louis-Schmid et al. 2007). Accordingly, organic production decreased, leading to enhanced oxygen content of seawater, which resulted in flourishing bioturbation by infaunal burrowers, and eventually led to better reservoir connectivity by burrows in the Ulayyah Member. Thus, the upward trends that show an increase of bioturbation from the base to top (from Hawtah to Ulayyah members) could be attributed to these first-order paleogeographic and paleoceanic controls.

Implications

The observations from outcrop and the constructed 3D models for TBN patterns and burrow intensity (Fig. 12B) provide a means to understand trends of reservoir connectivity in bioturbated strata. The

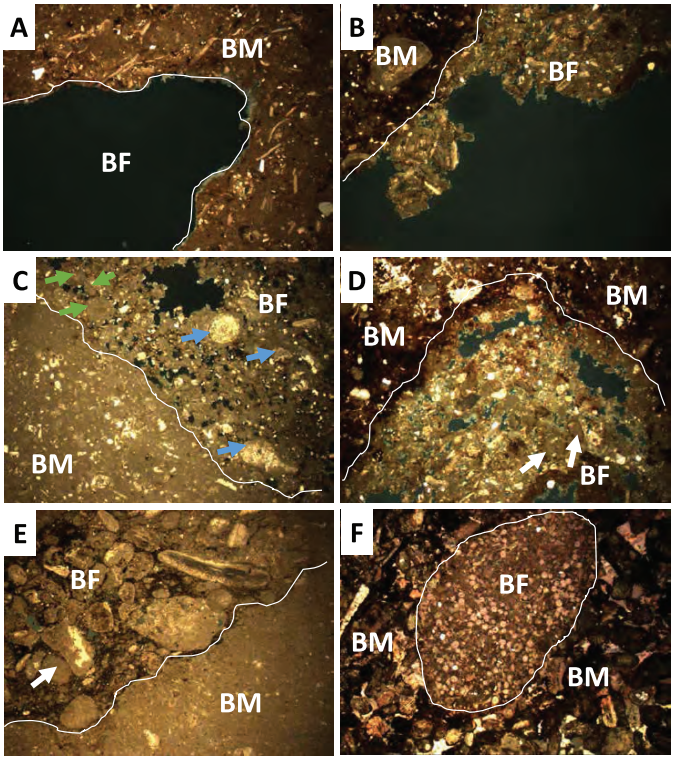

FIG. 10.—Thin-section photomicrographs of TBN pore systems showing burrow medium (BM) and burrow filling (BF) separated by the white lines (the width of the thin-section photomicrograph is ~1 mm): **A)** first pore type: open TBN with no filling, **B–E)** Second pore type, filled and partially filled TBN with estimated porosity of 10–20%; note that TBN filled with peloids (green arrows), skeletal grains (blue arrows), and coated grains (white arrows), **F)** third pore type: filled TBN with estimated porosity of 0%.

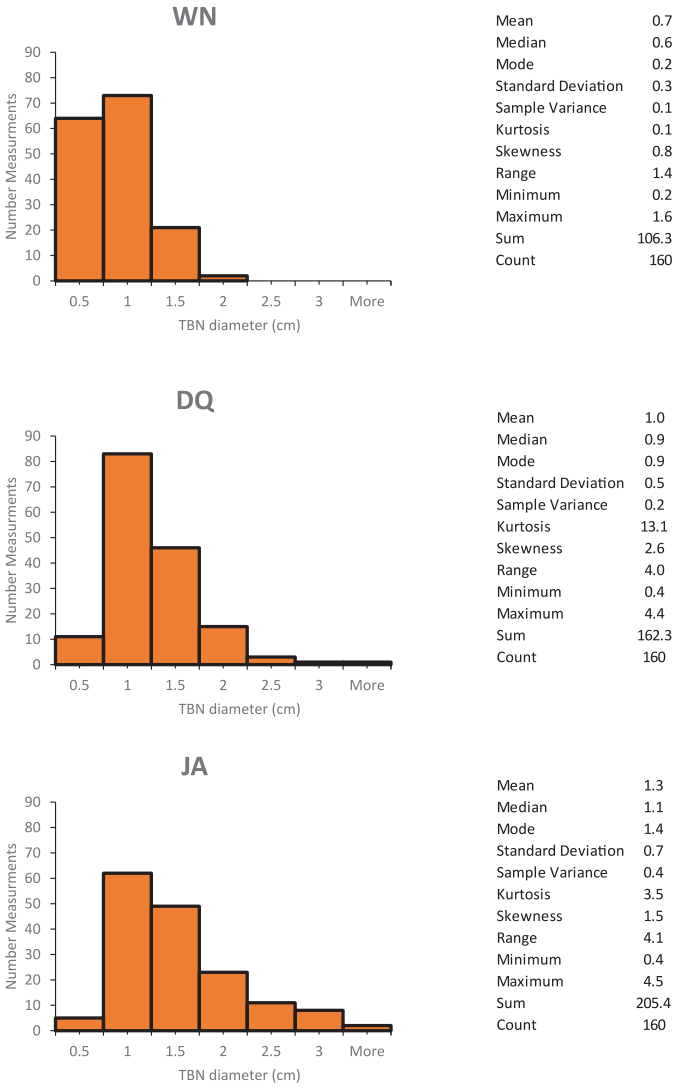

FIG. 11.—Histograms showing distribution of apparent burrow diameter in the three studied outcrops.

outcrop observations suggest two conditions in which TBN can contribute to reservoir connectivity and overall reservoir flow:

1. TBN beds overlie and are overlain by impermeable beds with poor reservoir quality (Fig. 7D, E). TBN-bioturbated beds can contribute to reservoir flow despite the beds above and below. In this case, the macropore system of TBN beds can provide excellent porosity and permeability, and even if the beds below and above the TBN beds are not permeable, the TBN beds can provide lateral flow in a vertical well.
2. TBN beds overlie and are overlain by grain-dominated beds with good reservoir quality (Fig. 7F). TBN bioturbated beds can breach the bed boundaries and thus connect above and below into more porous, more permeable grainy beds, providing overall reservoir connectivity for the carbonate reservoir and contribute to vertical and lateral flow.

These two conditions are also represented in the 3D model of burrow intensity of the TBN in the Hanifa Formation. In Figure 13, we show 2D slices from facies and burrow intensity 3D models, which represent the dip direction (depositional dip with respect to paleoshoreline) of these models. In these 2D slices, we placed three hypothetical wells (KICC 1–3) and extracted their synthesized facies and burrow intensity logs (Fig. 13C). There are three conditions in which TBN can contribute to reservoir connectivity based on the burrow intensity logs:

1. The intervals in KICC 2 and 3, marked by the black box, reflect the case in which TBN bioturbated beds can contribute to reservoir flow despite the beds above and below (similar to outcrop example in Fig. 7A, B).
2. The interval in KICC 1, marked by the green box, reflects the case in which beds overlie and are overlain by grain-dominated beds with good reservoir quality. TBN-bioturbated beds can breach the bed boundaries and connect above and below into more porous, more permeable grainy beds, providing overall reservoir connectivity (similar to outcrop examples in Fig. 7D–F).
3. The Ulayyah Member in the 2D slices and the three wells reflects the case in which TBN beds are juxtaposed with two compartmentalized, grain-dominated beds with interpreted good reservoir quality. TBN strata can provide reservoir connectivity for these otherwise laterally compartmentalized reservoirs and contribute to lateral flow.

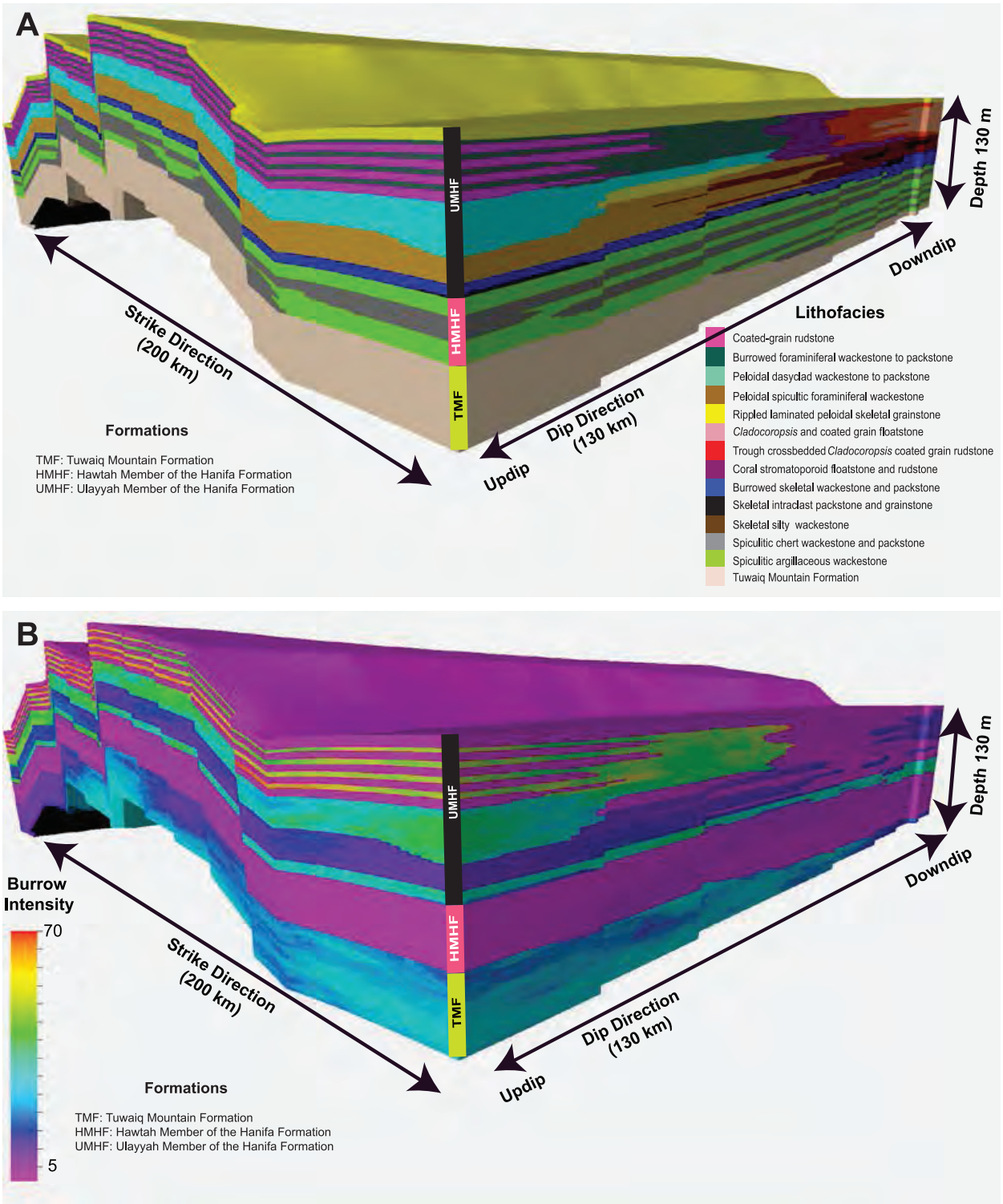

FIG. 12.—Constructed 3D models. **A)** Lithofacies models. **B)** Burrow intensity models. Models show variation in facies and burrow intensity in both strike direction (north–south direction) and dip direction (east–west direction) of the models.

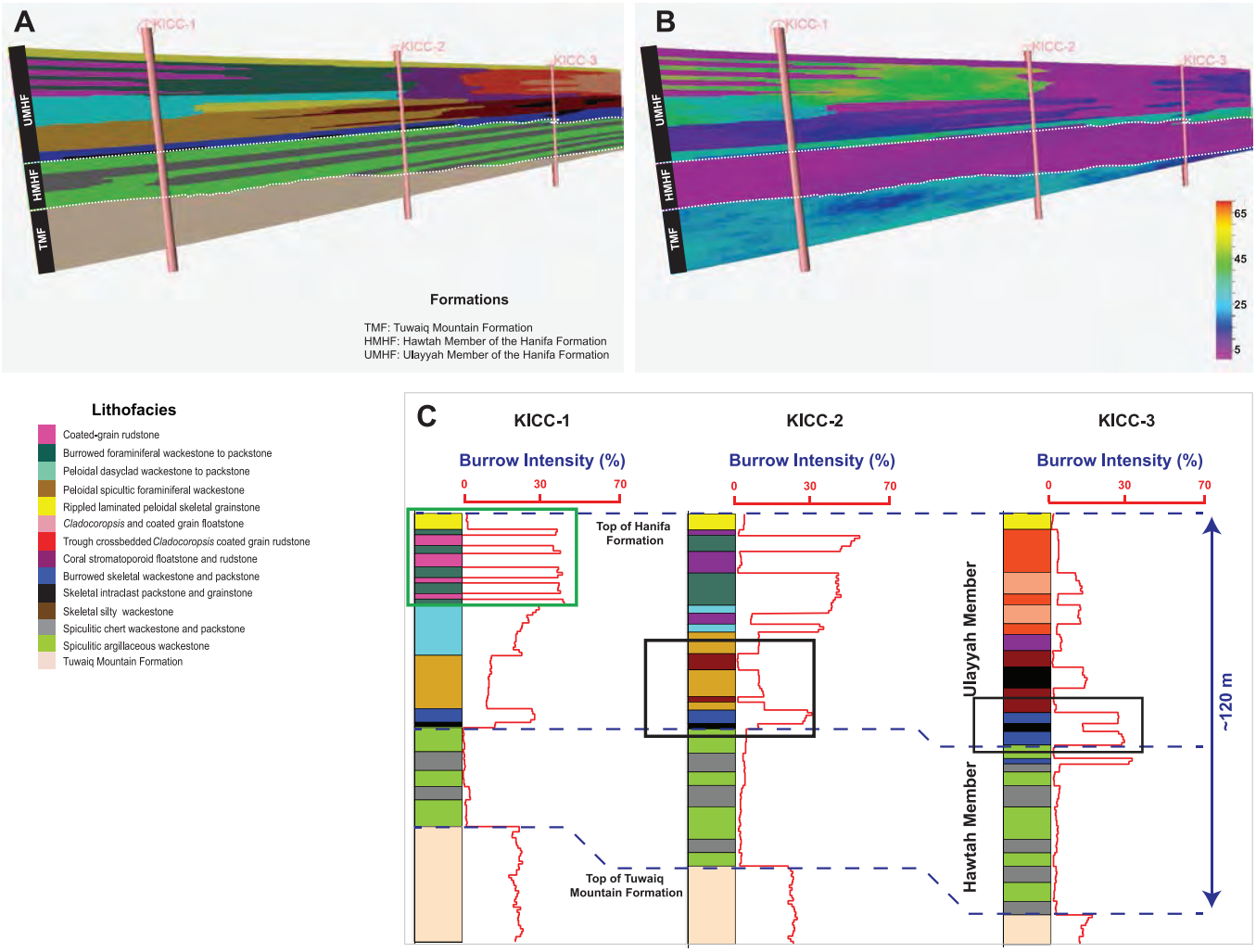

FIG. 13.—Pseudo-wells and their proposed facies and burrow intensity logs. **A)** 2D slices from the 3D lithofacies model. **B)** 2D slices from the 3D burrow intensity model. Note 2D slices show three proposed wells (KICC 1–3) placed on the 3D models. **C)** Extracted synthesized facies and burrow intensity logs for the KICC 1–3 wells. Note: The green and black boxes indicate intervals in which TBN have different flow properties (please refer to the text for explanation).

CONCLUSIONS

Strata of the Middle Jurassic Tuwaiq Mountain Formation and Upper Jurassic Hanifa Formation in central Saudi Arabia are highly bioturbated. Understanding bioturbation development in these strata is essential for understanding the lateral and vertical trends of preferred flow pathways associated with bioturbated carbonate in reservoirs close to the studied outcrops (e.g., Ghawar Field) and elsewhere in reservoirs with bioturbated carbonate. The main findings of this study are:

1. The pore systems of TBN in the Glossifungites Ichnofacies in the studied interval provide permeable pathways in the otherwise less permeable medium, suggesting vertical reservoir connectivity for carbonate strata.
2. In the 3D facies and burrow intensity models, TBN-bearing strata with ii2 to ii5 can be juxtaposed with grain-dominated lithofacies with interpreted good reservoir quality and provide lateral reservoir connectivity for otherwise compartmentalized reservoirs.
3. The controls on the spatial and vertical variability of the TBN can be attributed to changes in the water chemistry of the depositional environments, possibly linked to first-order, global paleogeographic and paleoceanographic conditions.

The findings obtained from this study are similar to several previous studies that showed the importance of bioturbation in improving reservoir quality. This study, however, used excellent, continuous exposures of outcrops as analogs that provide the basis for conceptual models to understand the spatial and temporal variations in bioturbation intensity in carbonated strata, and consequently, their lateral and vertical variations in flow properties. Such understanding is crucial for reservoir characterization, modeling, and enhanced oil recovery.

ACKNOWLEDGMENTS

We would like to thank all the sponsors of the Kansas Interdisciplinary Carbonates Consortium (KICC) for supporting this

study. Thanks to Mo'az Abd-Altwab, Mazin Bashari, Jarrah Mohammed, Mutasim Osman, Abdaseed Kubur and Husam Al-Zain from King Fahd University of Petroleum and Minerals (KFUPM) for assisting with the field works. Acknowledgments to Dr. Abdullah Al-Sultan from the Petroleum Engineering Department and Dr. Lameed Babalola from the Research Institute at KFUPM for the logistics and support they provide to host the investigators of this study at KFUPM campus during the field works, and for thin-sections preparation. We are grateful to Editors McNeill D, Harris PM, Rankey E, Hsieh J, and the anonymous reviewers who made critical suggestions to improve this paper.

REFERENCES

Alberti M, Fürsich FT, Pandey DK. 2012. The Oxfordian stable isotope record (δ18O, δ13C) of belemnites, brachiopods, and oysters from the Kachchh Basin (western India) and its potential for palaeoecologic, palaeoclimatic, and palaeogeographic reconstructions. *Palaeogeography, Palaeoclimatology, Palaeoecology* 344:49–68.

Al-Husseini MI. 1997. Jurassic sequence stratigraphy of the western and southern Arabian Gulf. *GeoArabia* 2:361–382.

Baniak GM, Gingras MK, Burns BA, Pemberton SG. 2015. Petrophysical characterization of bioturbated sandstone reservoir facies in the Upper Jurassic Ula Formation, Norwegian North Sea, Europe. *Journal of Sedimentary Research* 85:62–81.

Baniak GM, Gingras MK, Pemberton SG. 2013. Reservoir characterization of burrow-associated dolomites in the Upper Devonian Wabamun Group, Pine Creek gas field, central Alberta, Canada. *Marine and Petroleum Geology* 48:275–292.

Baniak GM, La Croix AD, Polo CA, Playter TL, Pemberton SG, Gingras MK. 2014. Associating X-ray microtomography with permeability contrasts in bioturbated media. *Ichnos* 21:234–250.

Bayet-Goll A, Samani PN, de Carvalho CN, Monaco P, Khodaie N, Pour MM, Kazemeini H, Zareiyan MH. 2017. Sequence stratigraphy and ichnology of Early Cretaceous reservoirs, Gadvan Formation in southwestern Iran. *Marine and Petroleum Geology* 81:294–319.

Cantrell D, Nicholson P, Hughes G, Miller M, Buhllar A, Abdelbagi S, Norton A. 2014. Tethyan petroleum systems of Saudi Arabia. *In* Marlow L, Kendall C, Yose L (Editors). *Petroleum Systems of the Tethyan Region*, Memoir 106: American Association of Petroleum Geologists, Tulsa, Oklahoma. p. 613–639.

Counts JW, Hasiotis ST. 2009. Neoichnological experiments documenting burrowing behaviors and traces of the masked chafer beetle (Coleoptera: Scarabaeidae: Cyclocephala sp.): Behavioral significance of extant soil-dwelling insects to understanding backfilled trace fossils in the continental realm. *PALAIOS* 24:75–92.

Cunningham KJ, Sukop MC, Huang H, Alvarez PF, Curran HA, Renken RA, Dixon JF. 2009. Prominence of ichnologically influenced macroporosity in the karst Biscayne aquifer: Stratiform "super-K" zones. *Geological Society of America Bulletin* 121:164–180.

De Wever P, O'Dogherty L, Goričan Š. 2014. Monsoon as a cause of radiolarite in the Tethyan realm. *Comptes Rendus Geoscience* 346:287–297.

Droser ML, Bottjer DJ. 1986. A semiquantitative field classification of ichnofabric. *Journal of Sedimentary Research* 56:558–569.

Droste H. 1990. Depositional cycles and source rock development in an epeiric intra-platform basin: The Hanifa Formation of the Arabian peninsula. *Sedimentary Geology* 69:281–296.

Ekdale AA, Bromley RG, Pemberton SG. 1984. *Ichnology—Trace Fossils in Sedimentology and Stratigraphy*, Short Course Notes 15: SEPM (Society for Sedimentary Geology), Tulsa, Oklahoma. 317 p.

Eltom H, Abdullatif O, Makkawi M, Abdulraziq A. 2014. Characterizing and modeling the Upper Jurassic Arab-D reservoir using outcrop data from central Saudi Arabia. *GeoArabia* 19:53–84.

Eltom HA, Gonzalez LA, Hasiotis ST, Rankey EC, Cantrell DL. 2018. Paleogeographic and paleo-oceanographic influences on carbon isotope signatures: Implications for global and regional correlation, Middle–Upper Jurassic of Saudi Arabia. *Sedimentary Geology* 364:89–102.

Eltom HA, Rankey EC, Hasiotis ST, Gonzalez LA, Cantrell DA. 2017. Impact of upwelling on heterozoan, biosiliceous, and organic-rich deposits: Jurassic (Oxfordian) Hanifa Formation, Saudi Arabia. *Journal of Sedimentary Research* 87:1235–1258.

Fallatah MI, Kerans C. 2018. Stratigraphic evolution of the Late Jurassic Hanifa Formation along the Tuwaiq Escarpment, Saudi Arabia: Evidence for a carbonate ramp system. *Sedimentary Geology* 363:152–180.

Gingras MK, Baniak G, Gordon J, Hovikoski J, Konhauser KO, La Croix A, Lemiski R, Mendoza C, Pemberton SG, Polo C, Zonneveld JP. 2012. Porosity and permeability in bioturbated sediments. *In* Knaust D, Bromley RG (Editors). *Trace Fossils as Indicators of Sedimentary Environments*, Developments in Sedimentology 64: Elsevier, Amsterdam. p. 837–868.

Gradstein FM, Gibling M, Sarti M, Von Rad U, Thurow J, Ogg JG, Jansa LF, Kaminski M, Westermann G. 1991. Mesozoic Tethyan strata of Thakkhola, Nepal: Evidence for the drift and breakup of Gondwana. *Palaeogeography, Palaeoclimatology, Palaeoecology* 88:193–218.

Halfen AF, Hasiotis ST. 2010. Downward thinking: Rethinking the "up" in soil bioturbation. *In* Gilkes RJ, Prakongkep N (Editors). *Proceedings of the 19th World Soil Congress*, Brisbane, Queensland, Australia. p. 21–24.

Hallam A. 2001. A review of the broad pattern of Jurassic sea-level changes and their possible causes in the light of current knowledge. *Palaeogeography, Palaeoclimatology, Palaeoecology* 167:23–37.

Hasiotis ST. 2002. *Continental Trace Fossils*, Short Course Notes 51: SEPM (Society for Sedimentary Geology), Tulsa, Oklahoma. 132 p.

Hasiotis ST, Mitchell CE. 1993. A comparison of crayfish burrow morphologies: Triassic and Holocene fossil, paleo- and neo-ichnological evidence, and the identification of their burrowing signatures. *Ichnos* 2:291–314.

Hasiotis ST, Platt B. 2012. Exploring the sedimentary, pedogenic, and hydrologic factors that control the occurrence and role of bioturbation in soil formation and horizonation in continental deposits: An integrative approach. *The Sedimentary Record* 10:4–9.

Hughes GW, Varol O, Al-Khalid M. 2008. Late Oxfordian micropalaeontology, nannopalaeontology and palaeoenvironments of Saudi Arabia. *GeoArabia* 13:15–46.

La Croix AD, Gingras MK, Dashtgard SE, Pemberton SG. 2012. Computer modeling bioturbation: The creation of porous and permeable fluid-flow pathways. *American Association of Petroleum Geologists Bulletin* 96:545–556.

La Croix AD, Gingras MK, Pemberton SG, Mendoza CA, MacEachern JA, Lemiski RT. 2013. Biogenically enhanced reservoir properties in the Medicine Hat gas field, Alberta, Canada. *Marine and Petroleum Geology* 43:464–477.

Leaman M, McIlroy D. 2017. Three-dimensional morphological and permeability modelling of diplocraterion. *Ichnos* 24:51–63.

Lindsay RF, Cantrell DL, Hughes GW, Keith TH, Mueller III HW, Russell SD. 2006. Ghawar Arab-D reservoir: Widespread porosity in shoaling-upward carbonate cycles, Saudi Arabia. *In* Harris PM, Weber LJ (Editors). *Giant Hydrocarbon Reservoirs of the World: From Rocks to Reservoir Characterization and Modeling*, Memoir 88: American Association of Petroleum Geologists, Tulsa, Oklahoma. p. 97–137.

Louis-Schmid B, Rais P, Bernasconi SM, Pellenard P, Collin P-Y, Weissert H. 2007. Detailed record of the mid-Oxfordian (Late Jurassic) positive carbon-isotope excursion in two hemipelagic sections (France and Switzerland): A plate tectonic trigger? *Palaeogeography, Palaeoclimatology, Palaeoecology* 248:459–472.

Meyer FO, Price RC, Al-Ghamdi IA, Al-Goba IM, Al-Raimi SM, Cole JC. 1996. Sequential stratigraphy of outcropping strata equivalent to Arab-D reservoir, Wadi Nisah, Saudi Arabia. *GeoArabia* 1:435–456.

Meyer FO, Price RC, Al-Raimi SM. 2000. Stratigraphic and petrophysical characteristics of cored Arab-D super-k intervals, Hawiyah area, Ghawar field, Saudi Arabia. *GeoArabia* 5:355–384.

Mitchell J, Lehman P, Cantrell D, Al-Jallal I, Al-Thagafy M. 1988. Lithofacies, diagenesis, and depositional sequence; Arab-D member, Ghawar field, Saudi Arabia. *In* Lomando AJ, Harris PM (Editors). *Giant Oil and Gas Fields*, Core Workshop Notes 12: SEPM (Society for Sedimentary Geology), Tulsa, Oklahoma. p. 459–514.

Pemberton SG, Gingras MK. 2005. Classification and characterizations of biogenically enhanced permeability. *American Association of Petroleum Geologists Bulletin* 89:1493–1517.

Powers R, Ramirez L, Redmond C, Elberg E. 1966. *Geology of the Arabian Peninsula*: US Geological Survey, Washington DC. Professional Paper 560. 147 p.

Reolid J, Betzler C. 2018. Ichnofabric logs for the characterization of the organic content in carbonates. *Marine and Petroleum Geology* 95:246–254.

Tonkin NS, McIlroy D, Meyer R, Moore-Turpin A. 2010. Bioturbation influence on reservoir quality: A case study from the Cretaceous Ben Nevis Formation, Jeanne d'Arc Basin, offshore Newfoundland, Canada. *American Association of Petroleum Geologists Bulletin* 94:1059–1078.

Wierzbowski H. 2002. Detailed oxygen and carbon isotope stratigraphy of the Oxfordian in central Poland. *International Journal of Earth Sciences* 91:304–314.